

Turbulent Superstructures in Inert Jets and Diffusion Jet Flames

Vadim Lemanov, Vladimir Lukashov and Konstantin Sharov *

Kutateladze Institute of Thermophysics SB RAS, Lavrentieva Ave. 1, Novosibirsk 630090, Russia;
lemanov@itp.nsc.ru (V.L.); luka@itp.nsc.ru (V.L.)

* Correspondence: sharov_konstantin@rambler.ru

Abstract: An experimental study of spatially localized very large-scale motion superstructures, propagating in a jet of carbon dioxide at low Reynolds numbers, was carried out. A hot-wire anemometer and a high-speed 2D PIV with a frequency of 7 kHz were used as measuring instruments. Such a puff-type superstructure in a jet with a longitudinal dimension of up to 20–30 nozzle diameters are initially formed in the jet source—a long tube in a laminar-turbulent transition mode (without artificial disturbances). It is shown that this regime with intermittency in time, when part of the time flow is laminar and the other part of time is turbulent, exists both at the exit from the nozzle and in the near field of the jet. Thus, the structural stability of such turbulent superstructures in the near field of the jet was found. Despite the large longitudinal scale, these formations have a transverse dimension of the order of several nozzle diameters. These structures have a complex internal topology, that is, superstructures are a conglomeration of vortices of different sizes from macroscale to microscale. Using the example of diffusion combustion of methane in air, it is demonstrated that in reacting jets, the existence of such large localized perturbations is a powerful physical mechanism for a global change in the flame topology. At the same time, the presence of a cascade of vortices of different sizes in the puff composition can lead to fractal deformation of the flame front.

Keywords: pipe gas jets; intermittent transition to turbulence; very large-scale motion; superstructures; puffs; autocorrelation function; diffusion combustion



Citation: Lemanov, V.; Lukashov, V.; Sharov, K. Turbulent Superstructures in Inert Jets and Diffusion Jet Flames. *Fluids* **2021**, *6*, 459. <https://doi.org/10.3390/fluids6120459>

Academic Editor: Tongming Zhou

Received: 15 November 2021

Accepted: 7 December 2021

Published: 16 December 2021

Publisher's Note: MDPI stays neutral with regard to jurisdictional claims in published maps and institutional affiliations.



Copyright: © 2021 by the authors. Licensee MDPI, Basel, Switzerland. This article is an open access article distributed under the terms and conditions of the Creative Commons Attribution (CC BY) license (<https://creativecommons.org/licenses/by/4.0/>).

1. Introduction

Beginning from the Refs. [1,2], coherent structures have become an essential part of jet flows. The use of such large vortices allows one to control heat and mass transfer processes and mixing processes in jet devices. The mechanism underlying the formation of large vortices was studied well enough [3,4], especially for jets issuing from contoured convergent nozzles for high Reynolds numbers ($Re > 10^4$). This geometry is due to the high practical importance of jets issuing from the nozzle. The initial velocity profile in this case is a top hat with thin shear layers. The laminar-turbulent transition in such flows develops in the mixing layer of the initial part of the jet ($x/d = 4-8$). Primary two-dimensional Kelvin-Helmholtz instability leads to the formation of vortices in the mixing layer. The pairing of such vortices and the secondary three-dimensional instability make the vortices increase up to the size of coherent structures in jet flows [5–8]. The main scenario responsible for the transition to turbulence in such flows involves the emergence of subharmonic oscillations [5,9]. Thus, large-scale motions appear in the initial part of the jet, and the characteristic cross-section scale of these motions is of the order of the mixing layer thickness [2,7]. Downstream, there are vortices with a size of the order of the jet cross-section [1,3].

It is known that jet flow dynamics depend essentially on initial conditions in inert and chemically reacting gases [10–12]. Nevertheless, jets issuing from tubes and holes have been much less studied. Almost no experimental data are available for such jets as far as velocity fluctuations at low Reynolds numbers are concerned. At the same time, long tubes are used in burners [11,13].

Currently, much attention is being paid to very large-scale motion superstructures [14,15]. Such large formations are observed both in forced convections in pipes and channels and in free convection flows [14]. The size of such vortices is $l/\delta \sim 10\text{--}20$ in near-wall boundary layers [16,17] and $l/d \sim 10\text{--}20$ in pipe flows [18–20]. According to our earlier research, large-scale structures appear not only in near-wall flows, but also in jet flows [21–23]. The vortices of such scales can be observed in the jets issuing from long axisymmetric channels at critical Reynolds numbers of 2000–3000. In this transitional range, the flow in a pipe is intermittent in nature [18,20]. This means that, in the time scale, the instantaneous flow velocity looks like intermittent regions of laminar and turbulent motion. Note that critical Reynolds numbers (Re_{cr}) in pipes are often derived from friction factors or heat transfer coefficients [24,25]. The Re_{cr} values depend on velocity distribution and the amplitude of inlet flow perturbations [20] and can be as high as 250,000 [26]. Local turbulent structures, puffs, appear at transition Reynolds numbers, and slugs are formed in turbulent flows [18,20]. The puffs are issued from a long pipe and move downstream to form superstructures $l/d \sim 20\text{--}30$ perturbing the jet [21–23].

Currently, the mixing and combustion of gaseous fuel jets is commonly controlled using coherent structures [27–29]. In this work, this approach is further developed for jet flames using turbulent superstructures formed during a laminar-turbulent transition inside long tubes. A contribution of this study is the use of a time-resolution PIV technique to obtain the velocity field information of puffs in jets. Turbulence superstructures have implications for constructing numerical models for calculating dynamics and heat transfer in the near field of inert jets and diffusion jet flames.

2. Experimental Setup

The experiments were carried out on installation, as shown in Figure 1. The working gas was supplied from a high-pressure gas vessel; the flow rate was controlled by a computer using a Bronkhorst El-Flow mass-flow meter (Bronkhorst High-Tech BV, Ruurlo, The Netherlands).

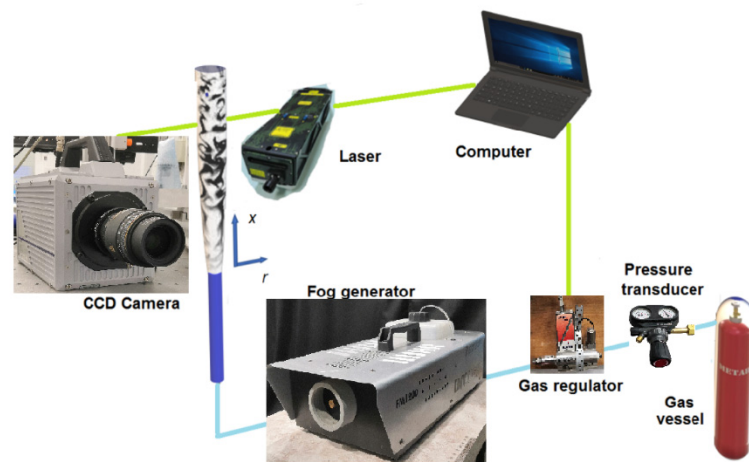


Figure 1. Experimental setup scheme.

The working gas was air and carbon dioxide (CO_2) in isothermal flows, and methane (CH_4 , 99.99%) in flame jets. Gaseous CO_2 was passed through a fog generator, where it was mixed with small (3–5 μm) glycerin droplets to visualize the flow, and supplied to the jet source in the form of a long round tube. The experiments with reacting flows were conducted without the use of a fog generator; instead, the working gas passed directly to the jet source.

In the case of isothermal CO_2 flow, an aluminum tube with an inner diameter of $d = 8$ mm and length of $L = 1.6$ m (i.e., $200d$) was used. The origin of coordinates coincided with the end of the tube, the axis x was directed downstream, and the r was measured

along the radius from the jet axis. In the case of PIV measurements of dynamic flow characteristics, the gas was supplied from a similar channel into a $400 \times 400 \times 400$ mm plexiglass flow-through passage. The reacting flows were studied using a brass tube with a diameter of 3 mm, a wall thickness of 0.5 mm, and a length of 1 m. A jet with an initial developed Poiseuille profile was formed at the tube outlet. In the experiments without combustion, the jet was visualized by a laser sheet using a Photonics DM high-speed pulsed laser (Photonics Industries International, Inc., New York, NY, USA), while the process of superstructure development was monitored using a high-speed camera. High-speed shooting was performed using a Photron SA5 camera with a 1 MPix matrix (Photron Ltd., Tokyo, Japan). The video was recorded with a frequency $f = 7$ kHz. The images from the high-speed camera were processed using Particle Image Velocimetry (PIV) techniques. As a result, instantaneous velocity fields were calculated and further used to obtain instantaneous velocity distributions over time along the axis and in the mixing layer. The reacting flows were recorded on Sony Alfa A6400 (SONY, Japan and Honor 10 (Huawei, Shenzhen, China) digital cameras. The jet with combustion was expanded in open-air space. Some experimental data were obtained on a DISA 55M hot-wire anemometer (DISA Elektronik A/S, Herlev, Denmark) using a DISA 55P11 sensor (DISA Elektronik A/S, Herlev, Denmark). During the experiment, no artificial disturbances were introduced either in the tube or in the jet. The inert jets were expanded in air at atmospheric pressure.

3. Results and Discussion

3.1. Inert Jets

In view of the fact that initial conditions play an essential role, much attention was paid to the flow state at the outlet of the cylindrical channel when studying inert free jets. Figure 2 shows the velocity ratio U_m/U_b and the turbulence degree ($Tu = u/U_m \times 100\%$) on the axis channel $r = 0$ mm as functions of the Reynolds number $Re = U_b d/\nu$ for $x = 0.5$ mm (U_m is the axial gas velocity at the tube outlet section, U_b is the bulk gas velocity in the tube, u is the root-mean-square value of velocity pulsations). As can be seen, the velocity ratio changes from $U_m/U_b = 2$ (corresponding to the laminar Poiseuille profile) to $U_m/U_b = 1.26$ (characteristic of a fully developed turbulent profile in a pipe). This change is due to the laminar-turbulent transition in the tube in the Re_1 – Re_2 range of 2395–2740. The turbulence degree Tu has a local extremum in the transition region at $Re = 2598$ where the maximum pulsation level $Tu = 14.7\%$ is reached. In this case, the intermittent regime (alternating laminar and turbulent flow regions) was observed.

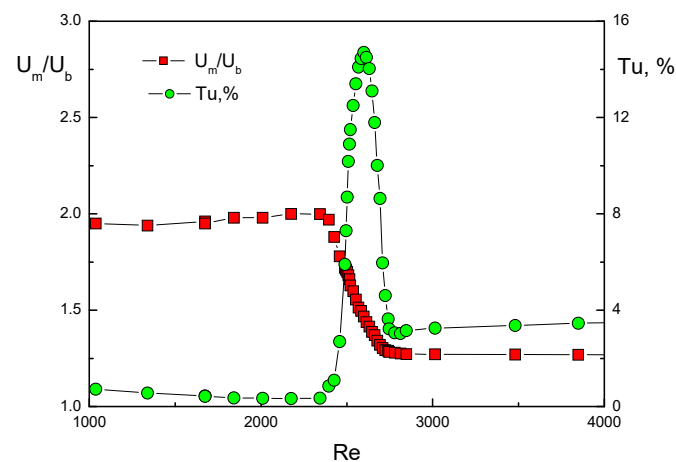


Figure 2. Velocity and velocity pulsations in the initial section of the CO_2 jet.

As is known, large-scale puff structures ($l/d \sim 10$ – 20) appear in the region of laminar-turbulent transition in pipes. However, there are almost no published facts of such large structures in jets observed in the literature. Our experiments demonstrated the existence

of such superstructures in jets. Figure 3 shows these data obtained by high-speed PIV at a frequency of 7 kHz. The obtained fields of instantaneous velocities made it possible to obtain time series of instantaneous velocity at any point in space within the working area. The velocity fields were exported to files containing the longitudinal and transverse velocity values for each vector of the instantaneous vector field, and the coordinates corresponding to this vector. Further, from these files, with the help of specially written programs, the time distributions of instantaneous velocities for points in space with given coordinates within the working area were extracted.

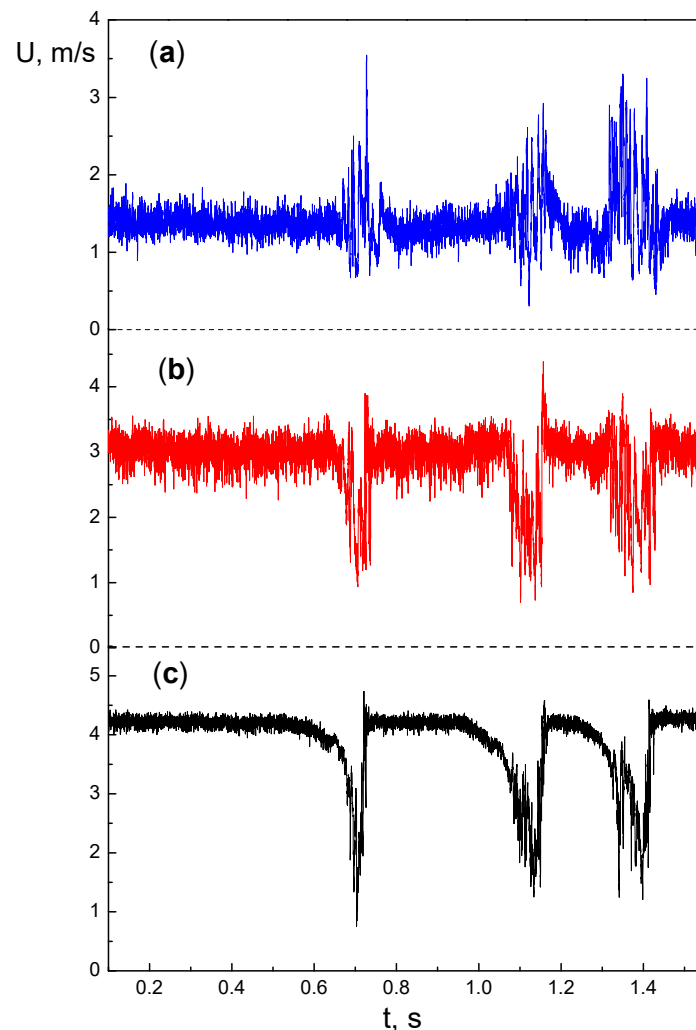


Figure 3. Time evolution of CO₂ longitudinal velocity in the mixing layer at distances $r = 4$ mm (a) and $r = 3$ mm (b) from the axis and on the axis ($r = 0$) (c) in the $x = 60$ mm cross-section for $Re = 2400$.

A total of 10,918 values were collected. Figure 3 presents three time series for the longitudinal velocity component for $x = 60$ mm on the jet axis ($r = 0$ mm) (a) and at distances $r = 3$ mm (b) and $r = 4$ mm (c) from the axis. All the three fragments were obtained for the same time interval $t = 1.6$ s by processing the working area (63×63 mm) in the laser sheet plane passing through the jet axis. In accordance with the studies of laminar-turbulent transition in channels [18,20], we classified these perturbations as puff structures.

Firstly, they were obtained in the range of Reynolds numbers corresponding to the laminar-turbulent transition inside a pipe. Secondly, all these axial velocity perturbations have high amplitudes, smooth leading fronts, and rather steep trailing fronts. Thirdly, no artificial perturbations were introduced in the tube or in the jet during the experiment. Comparing velocities on the axis with those at $r = 3$ – 4 mm reveals short-time correlations corresponding to the time instant of the puff passage. Thus, Figure 3 demonstrates the inter-

mittent flow character of the jet in the near field region and the presence of puff structures with extended longitudinal dimensions and relatively small transverse dimensions.

The most common phenomenon of intermittency occurs in two cases: (a) at the boundary of a turbulent boundary layer and an external laminar flow; (b) in the case of time-variable laminar-turbulent motion, for example, during flow in a channel [15,18,20]. In jet flows, the intermittency phenomenon is usually considered on the interface boundary where the turbulent jet flow alternates with the laminar part of the ejected surrounding gas [30,31]. In our study, we consider a flow that is intermittent with time at initial section of the jet stream (particularly, on the jet axis). The intermittency factor in the near field of the air jet issuing from a long tube ($d = 3$ mm, $L = 1$ m) was measured using a hot-wire anemometer. The intermittency factor γ was defined as the fraction of time when velocity fluctuations exceeded the threshold value. The γ value was estimated according to the procedure based on the time series of measured velocity [32]. The intermittency function was defined as: $\gamma = \frac{1}{T} \times \int_0^T I(t) dt$. Function $I(t) = 0$ if $D(t) \leq Th$ and the mode is laminar; $I(t) = 1$ if $D(t) > Th$ and the mode is turbulent, T is the length of time series data. Double differentiated velocity $D = d^2U/dt^2$ was used as a criterion function, and threshold level Th was defined by the “dual-slope method” [32].

The data in Figure 4 are presented on the axis for two coordinates: near the beginning of the jet ($x/d = 0.17$) and at distance $x/d = 20$. As can be seen from the Figure, the data for γ for different coordinates almost coincide for equal Reynolds numbers.

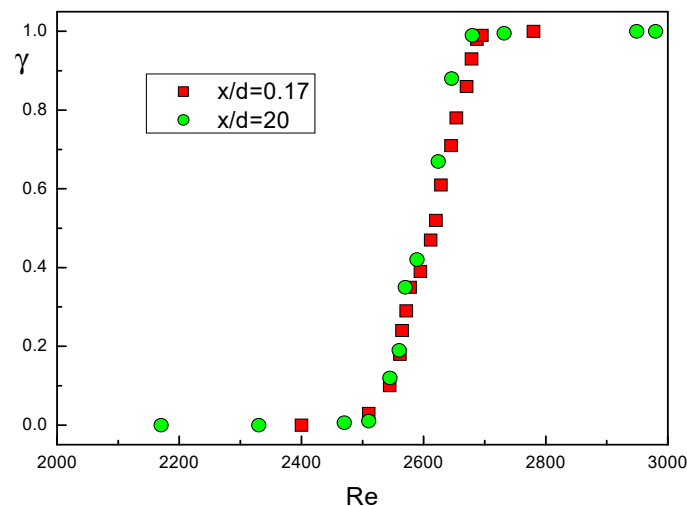


Figure 4. Intermittency factor in the air flow.

For the Reynolds number $Re_1 = 2500$, characterizing the lower boundary of the laminar-turbulent transition, the intermittency factor γ is close to 0, meaning that almost no localized turbulent structures appear. The level of velocity fluctuations in the cross-section $x/d = 20$ approximately corresponds to the maximum of pulsations at the exit cross-section of the pipe ($x/d = 0.17$, $Tu \sim 1\%$). The intermittency factor $\gamma = 0.5$ signifies that the flow is laminar for half the time and contains turbulent puff structures for the other half of the time. At a constant Reynolds number, the frequency of puff passage varies, that is, they pass one after another at random intervals. At the Reynolds number $Re_2 = 2690$, characterizing the upper boundary of the laminar-turbulent transition, the intermittency factor is $\gamma = 1$. The level of velocity fluctuations in the cross-section $x/d = 20$ also approximately corresponds to the maximum of pulsations at the exit cross-section of the pipe ($x/d = 0.17$, $Tu \sim 4\%$). In this case, the time series contains no laminar sections. Note, the Re_1 and Re_2 numbers in our experiments for air and methane differ. This is due to the fact that the critical Reynolds number for flow in pipes is very sensitive to the level of initial perturbations [18,20]. In these experiments, different gas lines were used (from the gas source to the tube inlet), while the level of disturbances at the tube inlet was not controlled. As can be seen from

the Figure 4, the data for γ for different coordinates almost coincide for equal Reynolds numbers. This conservative behavior of γ with variations in x/d can be explained by the structural stability of puff at the initial section of the jet. In our experiment, the breakup of such a disturbance occurs at $x/d > 20$.

Figure 5 shows instantaneous longitudinal velocities for a single puff on a short time interval of 0.6–0.8 s. The figure also presents three time series for $x = 60$ mm: on the jet axis for $r = 0$ mm (a) and for distances $r = 3$ mm (b) and $r = 4$ mm (c) from the axis. It is known [20] that the longitudinal velocity of puff structures in a pipe decreases to $\sim 0.6U_m$. As can be seen from the Figure, the velocity on the jet axis decreases to $\sim 0.25U_{cl}$. Comparison of the velocity values on the axis with those on the radius of 3–4 mm reveals short-time correlations at the time moment of puff passage. The level of velocity pulsations is much higher on the jet periphery than on the jet axis at time intervals before and after the puff passage.

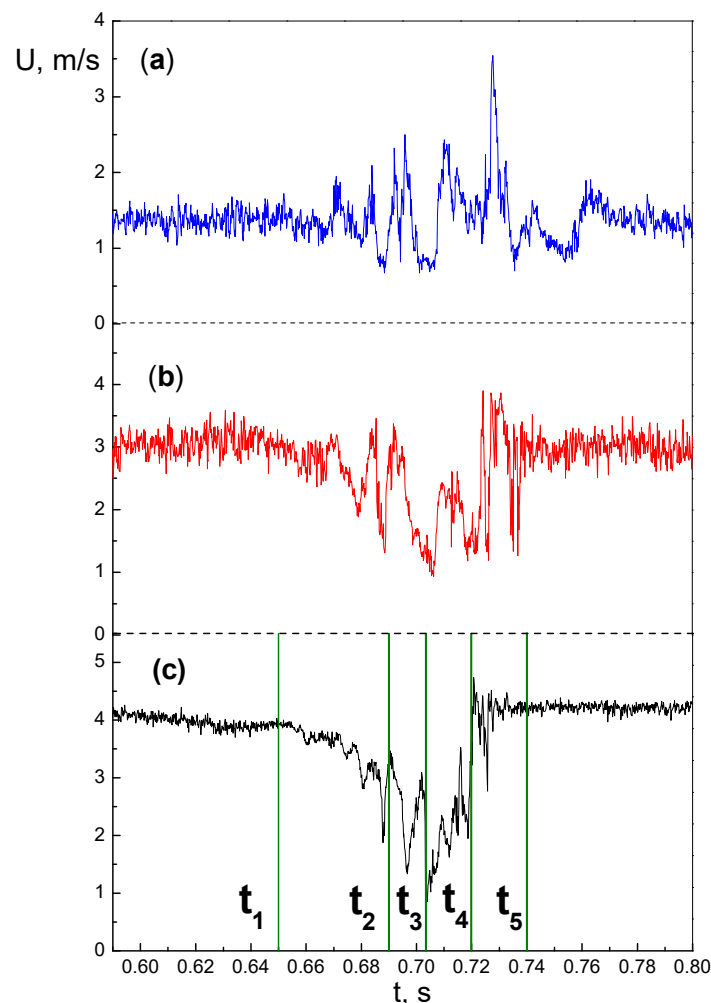


Figure 5. Time series of the single puff velocity in the mixing layer at distance $r = 4$ mm (a) and $r = 3$ mm (b) from the axis and on the axis ($r = 0$) (c) in the cross-section $x = 60$ mm (CO_2), $Re = 2400$. $t_1 = 0.65$ s; $t_2 = 0.69$ s; $t_3 = 0.7$ s; $t_4 = 0.72$ s; $t_5 = 0.74$ s.

This is due to the fact that the Kelvin-Helmholtz instability at the initial section develops in the mixing layer, and not on the axis of the jet. The leading front is smooth, while the trailing front is steeper. The analysis of time series at different distances from the axis shows that the trailing front in the mixing layer ($r = 4$ mm) follows slightly behind the similar front on the axis ($r = 0$). Note that the local extremum on the axis ($r = 0$) do not always correspond to the local extremum at the jet periphery ($r = 3$ – 4 mm).

All this indicates that the puff has a complicated internal spatial structure, in accordance with the data reported in the Ref. [25]. Apparently, the topology of such superstructures requires high-speed PIV tomographic research methods.

Using the high-speed PIV, we can trace the change in the spatial structure of the jet with a good temporal resolution ($\Delta t = 1/f = 143 \mu\text{s}$). The instantaneous velocity fields (a, c, e, g, i) and vorticity distributions (b, d, f, h, j) in the laser sheet plane (x, r), passing through the jet axis, are shown in Figure 6. Instantaneous vector fields of velocity $W = iU_x + jU_r$ are plotted, taking into account the velocity components (U_x, U_r); here, i, j are unit vectors along the (x, r) axes. These velocity fields are used to calculate the vorticity distribution in plane (x, r) by formula:

$$\omega = \left(\frac{\partial U_r}{\partial x} - \frac{\partial U_x}{\partial r} \right) \quad (1)$$

Gas moves upwards in the jet. The lower boundary in Figure 6 corresponds to the beginning of the jet; the field size is $63 \times 63 \text{ mm}$. The size of the tube outlet is shown graphically. The dynamic pattern (Figure 6) contains five time-fragments, which relate to the time series (Figure 5) of the process of one puff movement: (a) before the puff leaves the tube $1-t_1 = 0.65 \text{ s}$; (b) three options when the puff is in the measurement area ($t_2 = 0.69 \text{ s}$; $t_3 = 0.70 \text{ s}$; $t_4 = 0.72 \text{ s}$; and (c) when the puff leaves the measurement area ($t_5 = 0.74 \text{ s}$).

The first pair of figures (Figure 6a,b, $t_1 = 0.65 \text{ s}$) corresponds to the option when a disturbance is inside the tube and there is no puff in the measuring area. As it can be seen from Figure 6a, the near field of the jet consists of an axial core and a peripheral mixing layer.

In accordance with the velocity field, an almost vortex-free jet core is observed in Figure 6b. The Kelvin-Helmholtz instability, which leads to formation of a vortex motion, develops in the mixing layer. In this regard, maximum vorticity is concentrated in the mixing layer and has a symmetrical form relative to the jet axis, being divided into positive and negative parts. The length of the initial jet section, up to the zone where the mixing layers are closed and the transition to turbulence occurs, depends on the Reynolds number and can reach large values of the transition coordinate $x_1 = 200-300d$ at low Reynolds numbers [33]. In our experiment, the coordinate of the transition zone extended beyond our measurement region ($x/d = 8$). We did not perform the measurements in the region of transition to turbulence in this work.

The case when the puff structure moves down the jet within our measuring field is presented in three pairs of figures (Figure 6c–h). Due to the fact that the puff is characterized by a smooth leading edge [20], it is rather difficult to identify the beginning of the front in the velocity and vorticity fields. Two time-fragments $t_2 = 0.69 \text{ s}$ (Figure 6c,d) $t_3 = 0.70 \text{ s}$ (Figure 6e,f) correspond to the regime when the puff occupies the entire measurement area. At the time instant $t_2 = 0.69 \text{ s}$, the velocity fluctuations at the leading edge increase, and localized vortices become noticeable in the velocity field (Figure 6c). These vortices correspond to alternating positive and negative regions of vorticity concentration in the jet (Figure 6d). In the velocity fields (Figure 6c,e), a sinusoidal disturbance is observed in the axial region. This behavior of the puff core resembles the sin-mode characteristic of jets with a long initial section [1]. Time $t_3 = 0.70 \text{ s}$ reflects the maximum velocity decrease on the jet axis (see Figure 5) when the puff passes. As it can be seen from Figure 6e,f, vortex formation increases, the distribution of vortices becomes chaotic, and a noticeable increase in vortex motion in the transverse direction is observed.

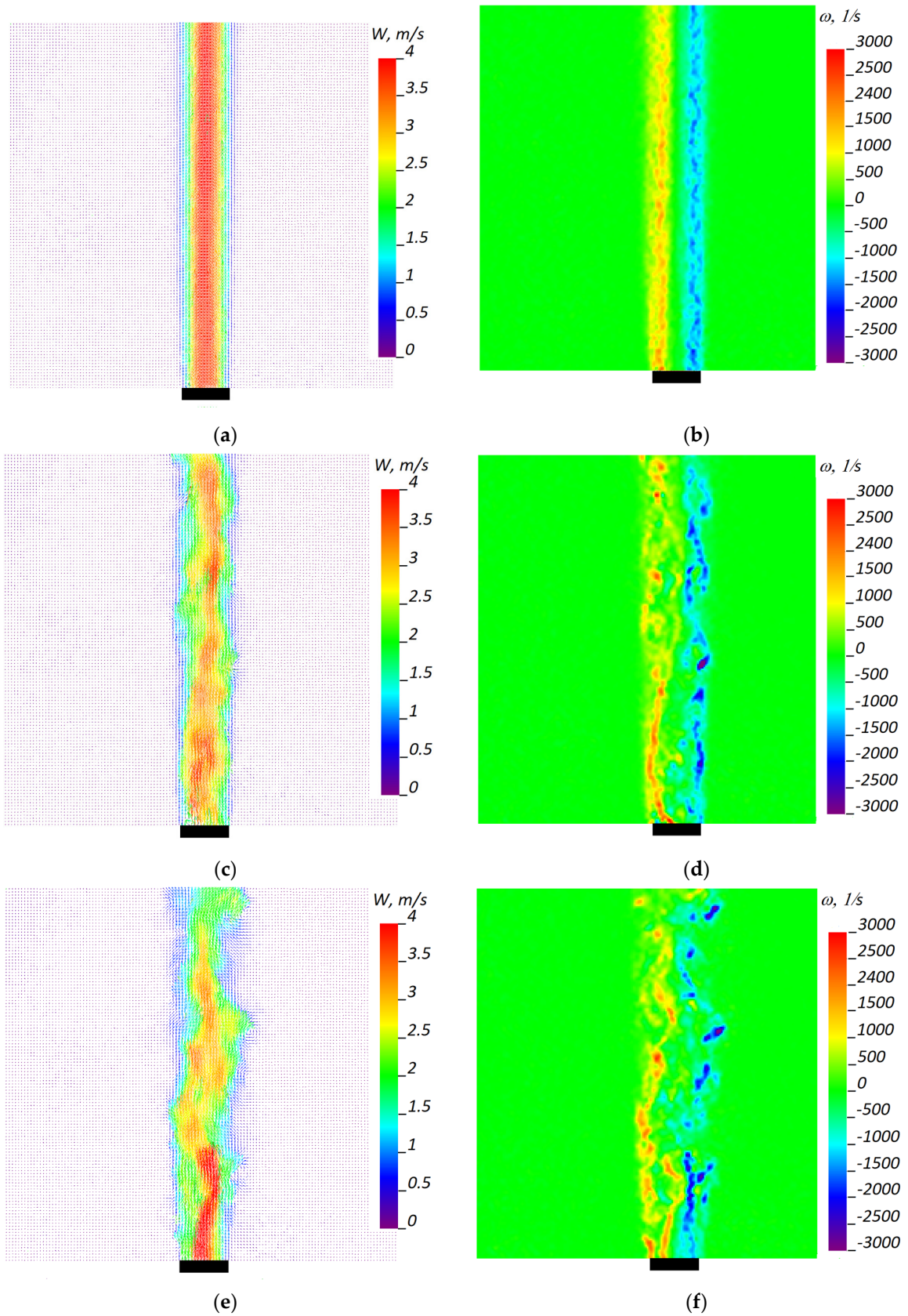


Figure 6. Cont.

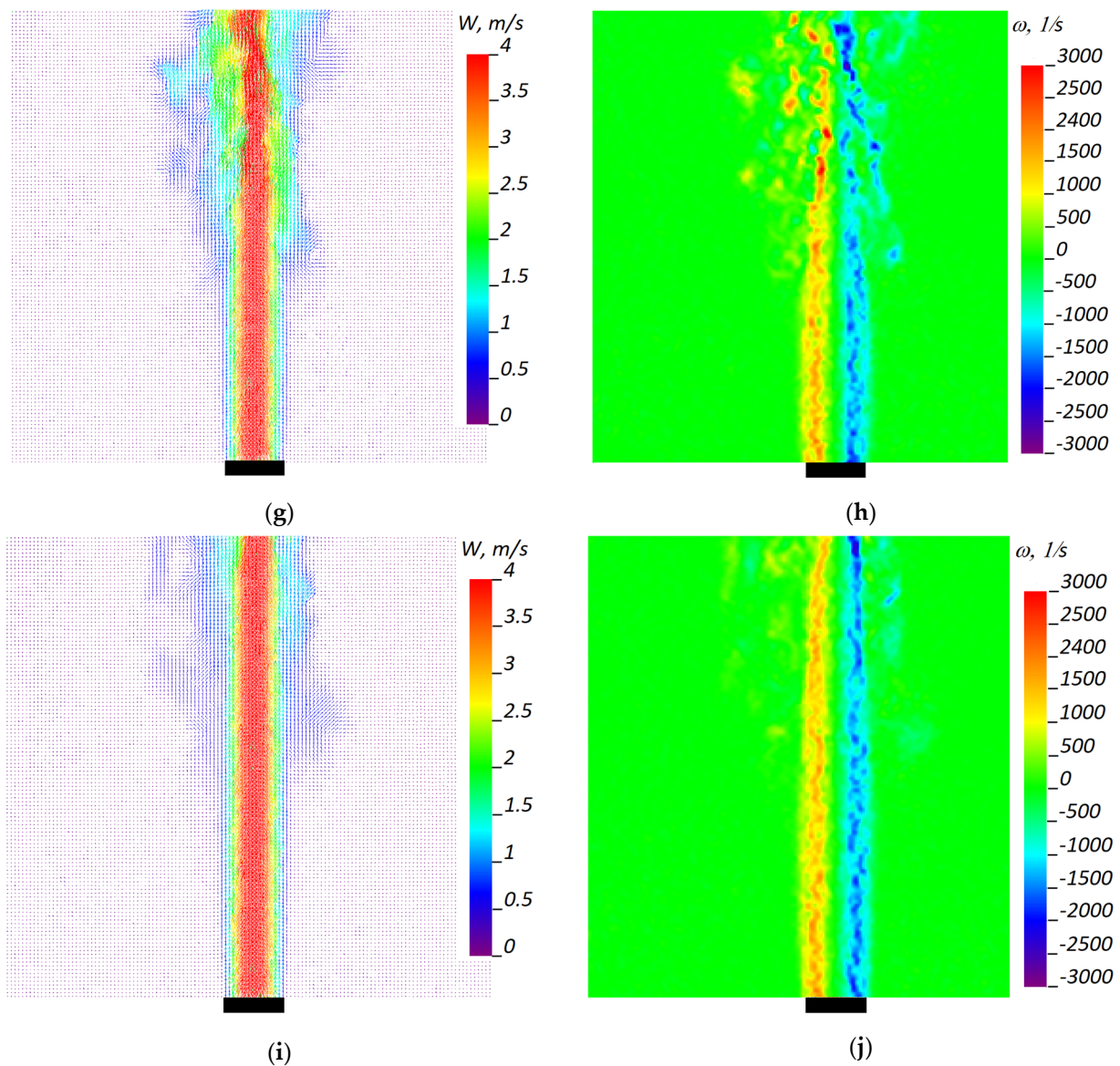


Figure 6. Instantaneous velocity (a,c,e,g,i) and vorticity (b,d,f,h,j) fields during puff propagation. The fields correspond to the time instants in the time series in Figure 5: (a,b) $t_1 = 0.65$ s; (c,d) $t_2 = 0.69$ s; (e,f) $t_3 = 0.7$ s; (g,h) $t_4 = 0.72$ s; (i,j) $t_5 = 0.74$ s.

Formation of the trailing edge of the puff ($t_4 = 0.72$ s) can be seen in the upper part of Figure 6g,h. The trailing edge of disturbance generates secondary vortices with a transverse size of about $3-4d$. Perhaps this explains the trailing edge “lag” at the jet periphery, observed when the trailing edge in the mixing layer ($r = 4$ mm) lags slightly behind the trailing edge on the axis in Figure 5. After trailing edge propagation through the velocity and vorticity fields (Figure 6g,h— $t_4 = 0.72$ s), it is clearly seen how the vortex motion region narrows. The lateral dimension reduces from $3-4d$ to $2d$ in the area where the puff is no longer present.

The last pair of figures (Figure 6i,j) corresponds to the case when the puff leaves the measurement field ($t_5 = 0.74$ s). The puff is located above the upper boundary of the figure; the velocity of its trailing edge is $\sim 0.25U_{cl}$, while the velocity of the oncoming undisturbed flow is $\sim U_{cl}$. It turns out that the undisturbed part of the jet somehow penetrates into the puff. Thus, Figure 6i,j demonstrates the end of the puff propagation and restoration of the laminar flow of the jet.

Further, the picture of the regime change is cyclically repeated in accordance with the time series shown in Figure 3. That is, the occurrence of puff-type structures in the

measurement region is randomly repeated. In this case, the probability of disturbance appearance corresponds to the intermittency coefficient shown in Figure 4.

As is known, statistical characteristics of dynamic processes include power spectrum and autocorrelation, which relate to completely different characteristics of the original signal. Autocorrelation reflects the memory and internal (temporary) relationships within the system, whereas the power spectrum refers to the dominating fundamental frequencies. The scenario of intermittent laminar-turbulent transition is characterized by the absence of dominating frequencies in the spectrum of velocity fluctuations [25,34]. In this regard, the autocorrelation function is the most interesting [35].

Figure 7 shows such data plotted for the longitudinal component of velocity pulsations in the case of turbulent flow ($Re = 3077 > Re_2$) and for single puffs ($Re = 2400 > Re_1$). As can be seen, the characteristic time for single puffs significantly exceeds that for the turbulent flow. This indicates that the longitudinal size of such structures during laminar-turbulent transition is significantly larger than characteristic structures in the turbulent flow, thus justifying the use of the term “superstructure” for large turbulent puff formations. The data for the turbulent flow show a monotonic decrease of $R(\tau)$ with a small negative part, which is typical of developed turbulent flows. The spatial integral scales of longitudinal structures l can be estimated using the Eulerian integral time scale $t^* = \int_0^\infty R\left(\frac{\tau U_{cl}}{d}\right) d\left(\frac{\tau U_{cl}}{d}\right)$ calculated according to the data in Figure 7. This integral for a turbulent flow is $l/d = t^* \times U_{cl}/d = 0.04$. The longitudinal puff scales for variants 2–4 are $l/d = 15, 28,$ and 25 . Function $R(\tau)$ for the same laminar flow (not shown) is that of a noise giving the limitations of our PIV measurements [36].

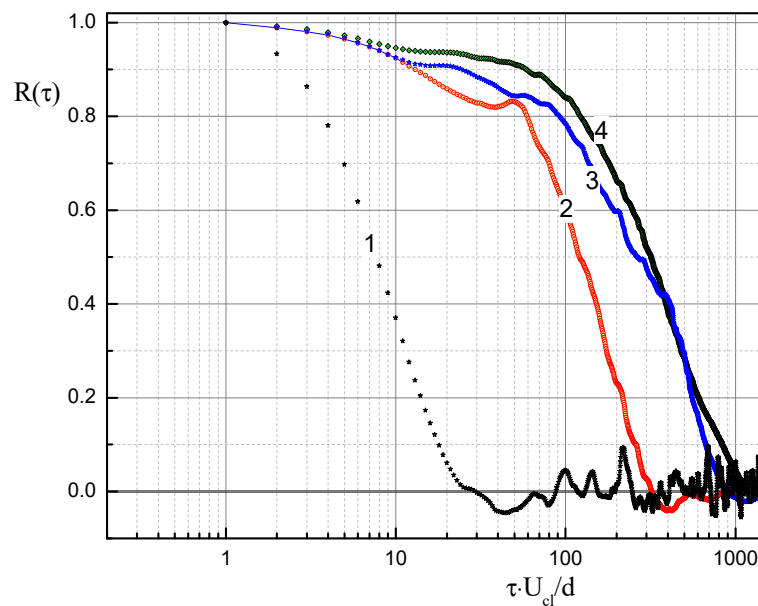


Figure 7. Autocorrelation function on the jet axis in the section $x = 60$ mm (CO_2): turbulent flow (1), and autocorrelation characteristics of single puffs (2–4).

According to the measurement results, the near field region of the jet ($x/d < 40$) in the range of Reynolds numbers corresponding to the laminar-turbulent transition in the pipe can be conditionally divided into two stages in time (Figure 8). In the “laminar” stage at $Re < Re_1$, the flow (Figure 8a) qualitatively corresponds to the pattern of a jet issuing from a convergent nozzle. In the initial zone 1, the Kelvin-Helmholtz instability develops in the mixing layer and leads to the formation of a vortex motion. The length of zone 1 (Figure 8a) depends on the Reynolds number, and the transition coordinate can reach values as large as $x_1 = 200\text{--}300d$ for small Reynolds numbers $Re = 300\text{--}400$ [33]. Further downstream, there is a turbulent zone 2. In this case, the velocity profile and the distribution of velocity

pulsations are similar to those observed in turbulent jets at large Reynolds numbers. In the “turbulent” stage of the flow, the superstructures prevail (Figure 8b) due to the fact that firstly, their longitudinal size can reach $20\text{--}30d$, that is, it greatly exceeds the structures typical of the instability development in the mixing layer (\sim thickness of the mixing layer). Secondly, their level of velocity pulsations is an order of magnitude higher than that in the mixing layer in the “laminar” stage. Note that the length of the zone before the transition to turbulence x_1 significantly depends on the Reynolds number and is equal to $x_1 = 10\text{--}15d$ when a laminar-turbulent transition occurs inside the pipe. Thus, during the “turbulent” stage, the puff occupies the entire zone 1. The measured time series of instantaneous velocities at this point show residual turbulent spots, increasing instability of Kelvin-Helmholtz waves, and an overall increase of broadband noise. The preliminary experiments indicate that puffs are destroyed in zone 2, but the mechanism of their decay requires additional research.



Figure 8. Two jet flow stages in the laminar-turbulent transition regime: (a) the “laminar” stage, (b) the “turbulent” stage.

3.2. Diffusion Jet Flames

Analysis of flame/vortex interactions is important for the development of turbulent combustion models and combustion stability models [27]. One such model represents the turbulent flame by the interaction of a laminar, non-premixed flame with repeatable toroidal vortices [37]. In our case, the repeatable vortices are the puff structures. As it was shown earlier [21,23], the scenario of disturbance development in a diffusion flame is the same as that for puff structures in a free isothermal jet. The range of Reynolds numbers also corresponds to the intermittency scenario of laminar-turbulent transition in the supply tube. In the absence of artificial disturbances in the channel, the appearance of puff structures in the flame is probabilistic in nature. As is known, some of the structures completely decay inside the tube [19]. Large vortex structures ($l/d \sim 20\text{--}30$) are localized in the near-axis region of the fuel jet. Its transverse size is of the order of the nozzle diameter in the laminar zone and notably larger in the turbulent zone. The presence of superstructures significantly affects the behavior of the flame front. The effect of puffs on the reacting flow depends on the type of torch (attached, detached flame) and on fuel mixture components. For example, the front of the attached propane flame is only slightly affected by the disturbance of the near-axis fuel region by puffs [21,23].

The results for the reacting jet were also obtained for the intermittent regime in the $Re_1\text{--}Re_2$ range for the Reynolds number $Re = 2312$. The gas flow passed from the bottom to the top. The time video sequence was taken from a single prolonged record. Figure 9a shows the image of an unperturbed attached diffusion flame of methane without puffs. Using a photo flash allowed obtaining a twin image similar to the schlieren image of the flame against a white screen. The left side of the figure contains two bright flame regions, apparently due to the glow of soot particles. The flow pattern is qualitatively similar to the results reported in the Ref. [13] for diffusion flame jets of hydrogen flowing out of a long tube. The laminar fuel jet core propagates in the interval of length $x/d \sim 26$ up to point A corresponding to coordinate x_1 for the inert gas jet. After point B, the regime of turbulent fuel flow develops. In this region, the laminar flame transforms into the turbulent flame; as a result, the flame cross-section significantly increases and an intensely glowing red region

appears. Such flow structure is almost stationary, with the exception of positions of points *A* and *B* which vary slightly. As it was mentioned in the Ref. [38], the transition from laminar to turbulent flame jets significantly depends on the composition of the combustion gas.

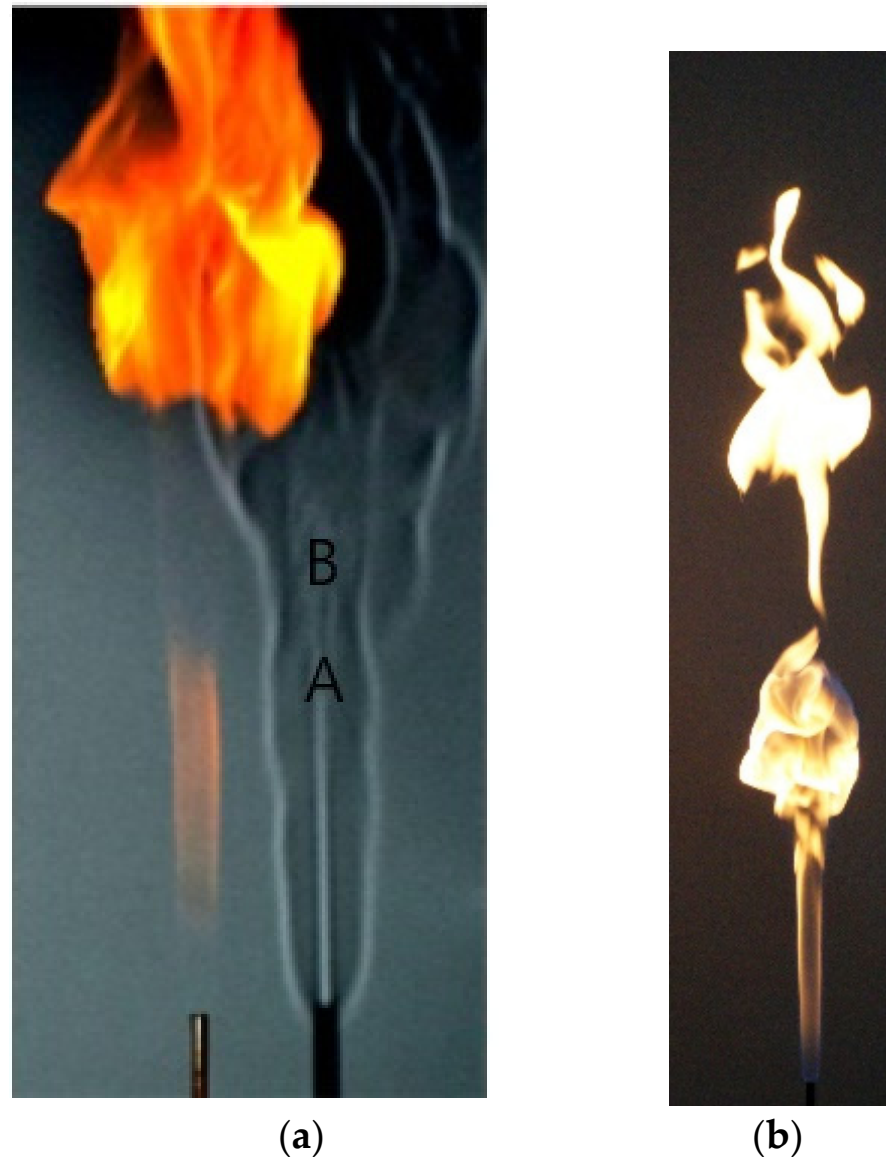


Figure 9. Methane diffusion flame, $Re = 2312$, $d = 3$ mm, $L = 1$ m. Unperturbed flow (a), emanation of puffs (b).

Figure 9b shows the effect of the puff on the flame structure. As can be seen from the images of the attached methane-air flame, the flame topology is significantly affected by the puff passage. The bottom of Figure 9b shows the laminar section and the puff superstructure followed by local extinction and the traces of the previous flame section.

Figure 10 shows a more detailed sequence of video frames presenting the puff passage dynamics. The total length of the undisturbed flame is about 240 mm for the mass-averaged jet velocity 15.5 m/s. The first changes in the flame shape due to the puff passage appear in frame 79. Having a characteristic longitudinal size of $\sim 30d$, the puff structure takes 3 frames that were recorded at a speed of 480 fps (Figure 10, frames 79–81). The disturbance caused by the laminar-turbulent transition maintains at much larger times scales (frames 79, 85) and may be associated with local extinction and formation of spatially separated combustion regions (frames 84, 85).

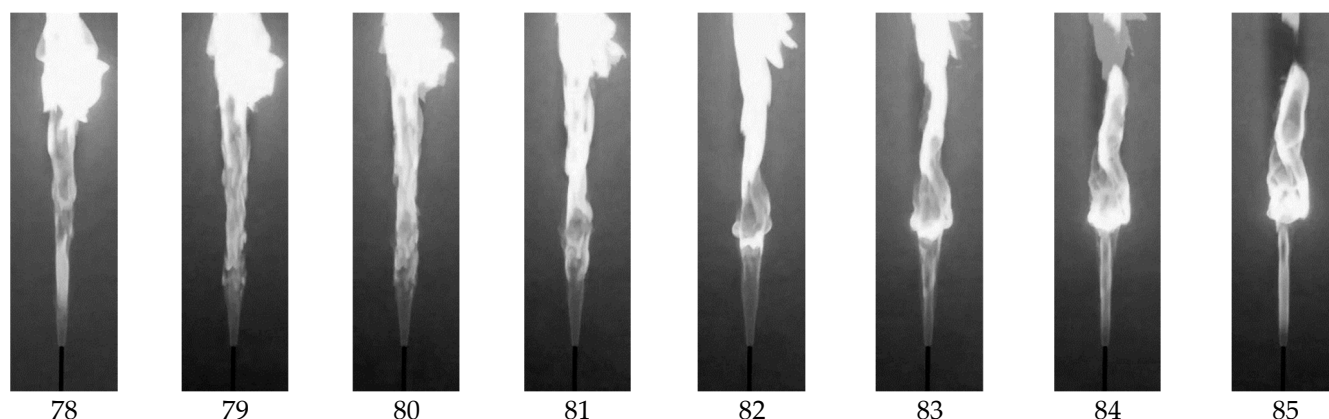


Figure 10. Sequence of video frames (480 fps) of vortex disturbance in the methane–air flame. Frame numbers 78–85, $Re = 2312$, $d = 3$ mm (see Supplementary Materials).

It is known that a methane diffusion flame issuing from a tube of small diameters $d = 1–3$ mm exists only in the regime of an attached flame [39]. In contrast to propane–air flames, increased fuel consumption upon methane combustion leads only to flame blow-off and extinction. In our experimental conditions ($d = 3$ mm, $Re = 2312$), the methane–air flame remained attached under the influence of puff structures, and no combustion blow-off was observed.

As is known, the dynamics of reacting jets depends on numerous factors, such as gas properties, fuel mixture, and burner geometry. However, our experiments showed that the disturbance development in the near field region of the fuel jet is similar to the inert jet with puff structures. The characteristic superstructure scales in the reacting jet are the same as those in the inert jet at the Reynolds numbers corresponding to the laminar–turbulent transition in the tube. Apparently, the effect of disturbance on the flame front is determined by the proportion of several main factors: density gradient in the radial direction, deformation of the flame front, and velocity of flame propagation. The presence of superstructures is a strong physical mechanism causing profound changes in the flame topology. At the same time, the presence of a cascade of different size vortices inside the puff can cause fractal deformation of the flame front. These two mechanisms are promising in terms of diffusion flame control.

It can be seen that there is a significant deformation of the flame, accompanied by a violation of the symmetry of the reacting flow. Note that these two chemical systems are very similar. The values of the quantities characterizing the flame—the flame propagation velocity, the characteristic thickness of the reaction zone, and the flame temperature—are quite close. In the diagram of the diffusion flame Figure 7, it can be seen that these systems practically coincide. Apparently, the density gradient in the radial direction for a thermally stratified flow may be a significant factor determining the flame stability. Assumingly, if the Richardson number $dRi/dr < 0$ and the radial temperature gradient $dT/dr < 0$, then the stratification is unstable (methane–air flame).

As it can be seen from Figure 10, when methane burns in the presence of a puff, significant deformation of the flame front, accompanied by violation of the symmetry of the reacting flow, occurs. At the same time, as our experiments show [21], the attached propane–air flame is deformed insignificantly. At that, the values of the parameters characterizing these two cases (flame propagation velocity, characteristic thickness of the reaction zone, and flame temperature) are quite close. To describe interaction of concentrated vortices with a diffusion flame front, the diagram [40] shown in Figure 11 can be used. In this paper, large-scale puff-type structures are proposed to be considered as concentrated vortices. In Figure 11, $P = l_t/\delta_L$ is the linear scale ratio, and $S = \frac{u_t}{S_L}$ is the characteristic velocity ratio. Here l_t is the characteristic longitudinal scale of turbulent velocity pulsations, δ_L is the thickness of the flame front, u_t is the characteristic of velocity

pulsations, S_L is the flame propagation velocity. As it is shown above, the puff-type vortex structures in a flame have a complex internal structure. In addition, it should be taken into account that the dynamics of disturbance development in the axial and radial directions is substantially anisotropic. Apparently, the density gradient in the radial direction for a thermally stratified flow can be a significant factor determining the flame stability. It is known that in stratified flows, a decrease in the Richardson number $Ri = \Delta\rho g l / (\rho_0 U_b^2)$ leads to turbulence intensification [41]. The outflow of a denser gas (for example, $\rho_{C_3H_8} = 2.1 \text{ kg/m}^3$) into a less dense ($\rho_{air} = 1.2 \text{ kg/m}^3$) medium allows instability suppression and an increase in the length of the jet laminar part due to the density gradient [42]. Conversely, when a jet of a lighter gas is injected (for example, $\rho_{CH_4} = 0.75 \text{ kg/m}^3$), an increase in the flow disturbance in the radial direction can be expected. If we take l (the longitudinal size of the puff) as l_t , the values of P and S for methane and propane correspond to the Weak Flame Wrinkling region in the diagram. The corresponding points in the diagram shown in Figure 11 almost coincide with each other.

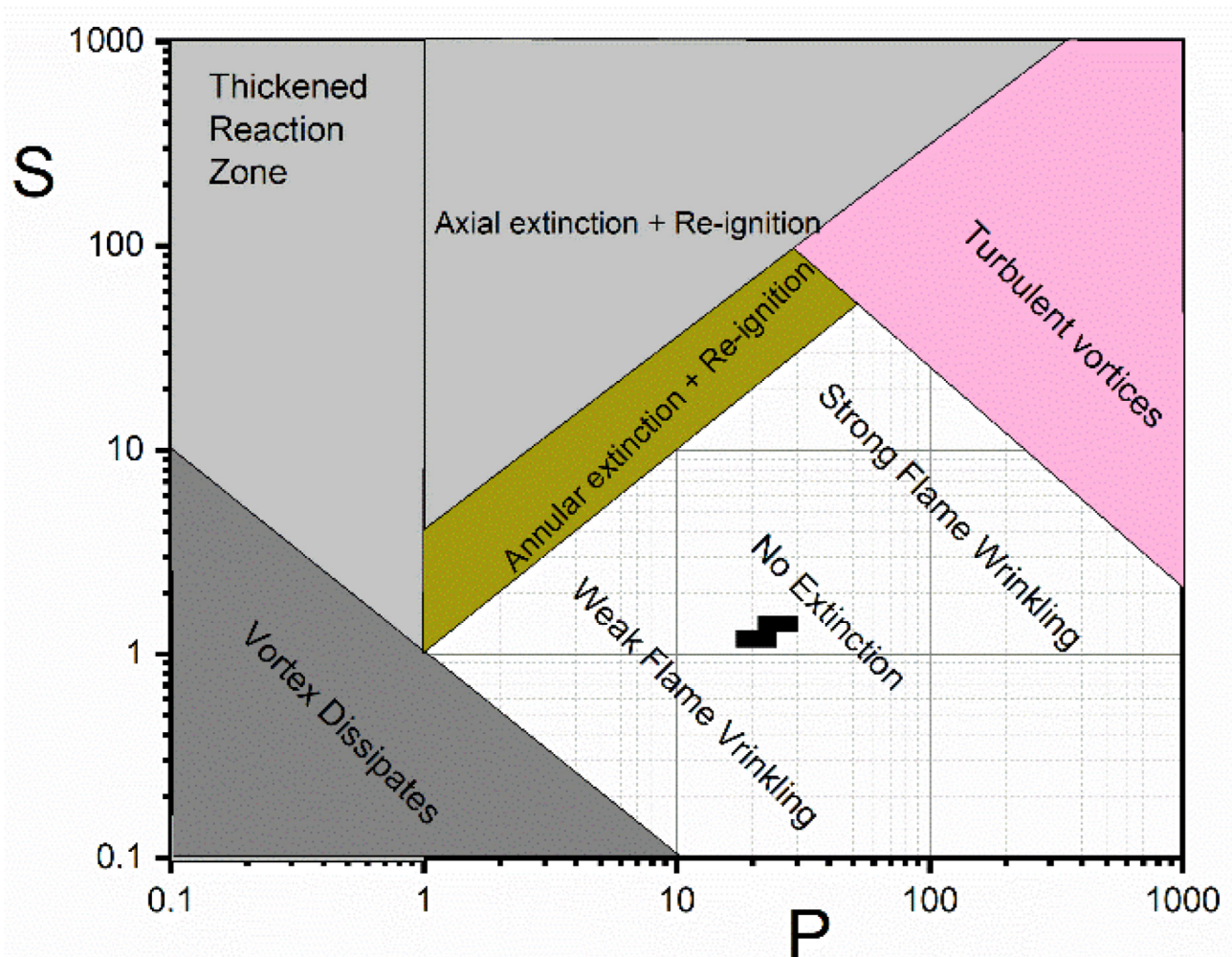


Figure 11. Diagram for non-premixed flame/vortex interactions [40]. Black marks: higher-methane, lower-propane.

4. Conclusions

The paper presents an experimental study of subsonic flows in the near field of inert and reacting circular jets. The jets flowed from long axisymmetric channels with a diameter of 3–8 mm into air at low Reynolds numbers of 2000–4000. The following fluids were used as a working liquid: for inert jets, it was air and carbon dioxide (CO_2), and for reacting jets, it was methane (CH_4). Gas jets flowed into air at atmospheric pressure. During the experiment, no artificial disturbances were introduced both in the tube and in the jet.

A hot-wire anemometer and a high-speed 2D PIV were used to diagnose the flow. For non-reacting jets, the distribution of the average velocity and velocity pulsations in the initial section (CO_2), and the intermittency coefficient in the initial cross-section ($x/d = 0.17$) and at distance $x/d = 20$ (air) were measured. The main emphasis was placed on the PIV measurement of velocity fields with a frequency of 7 kHz in a plane passing through the jet axis with a measurement area of 63×63 mm, which included the beginning of the CO_2 jet. For a reacting methane jet (CH_4), the diffusion flame was visualized in the regimes of a laminar-turbulent transition inside a long round tube.

The following main results were obtained in the research:

1. In accordance with the universal scenario of laminar-turbulent transition through intermittency, a two-stage pattern of a subsonic gas jet flow from long tubes in the near region was proposed. This pattern refers to Reynolds numbers, when a laminar-turbulent transition occurs inside the jet source (a long tube) and large-scale puff structures are formed. At the “laminar” stage, there is no puff in the near region of the jet, and at the “turbulent” stage, the puff is available.
2. According to the measurements of the intermittency coefficient in an inert jet, the data for different coordinates ($x/d = 0.17$ and at distance $x/d = 20$) almost coincide at $Re = idem$. This indicates that, on the whole, the puff structure is sufficiently stable and conservative in the near field of the jet up to the zone of transition to turbulence.
3. Based on the velocity fields measured by the high-speed PIV, the time autocorrelation function on the jet axis in cross-section $x/d = 20$ was determined. The spatial integral scale in a turbulent flow at $Re = 3077$ is $l/d = 0.04$. At the same time, the longitudinal scale of a puff at $Re = 2400$ is $l/d = 9\text{--}23$, and this justifies the use of the term “superstructure” for turbulent puff formations.
4. The results of measuring the flow field using high-speed PIV allowed us to establish that the puff is characterized by complex temporal and spatial dynamics. At the “laminar” stage, in the initial section, there is a vortex-free core near the jet axis and large vorticity in the mixing layer of the jet caused by the Kelvin-Helmholtz instability. At the stage of superstructure propagation, it is possible to diagnose a disturbance extended along the x -axis ($20\text{--}30d$) with a smooth leading and steep trailing edges. In addition, the level of velocity fluctuations increases noticeably, which increases vorticity in the entire puff region. Second, at the moment of a maximal decrease in the velocity on the jet axis to a value of $\sim 0.25 U_{cl}$, a sinusoidal disturbance is observed in the axial region of the puff, which leads to formation of localized vortices. Downstream, the dynamics of these vortices becomes more chaotic. Intense vortex formation leads to a significant increase in the jet in the radial direction up to values of $3\text{--}4d$.
5. The two-stage flow pattern also takes place in the near region of the reacting gas jet flowing out from long tubes. It was found that the presence of a chemical reaction can make a significant addition to this mechanism. It is shown that during methane combustion, the puff movement leads to a significant deformation of the flame front, and at the same time, during the propane flame combustion, the deformation of the front is less significant. For the first time, the P - S diagram [40] was used to describe the interaction of large-scale puff vortices and the flame front of methane and propane. It was found that the location of methane and propane on the diagram corresponds to the “Weak Flame Wrinkling” region. The formation of superstructures can be the determining mechanism for a global change in the flame topology. Thus, the presence of vortices of different sizes in the puff composition can lead to fractal deformation of the flame front. These mechanisms provide a basis for the formation of a new method for controlling diffusion combustion in devices using long tubes and channels.

Supplementary Materials: The following are available online at <https://www.mdpi.com/article/10.3390/fluids6120459/s1>.

Author Contributions: V.L. (Vadim Lemanov), V.L. (Vladimir Lukashov), and K.S. have equally contributed to the development of the present paper, including the conceptualization, methodology, data acquisition and analysis, interpretation of the results, and manuscript preparation. All authors have read and agreed to the published version of the manuscript.

Funding: This research was funded by Ministry of Science and Higher Education of the Russian Federation, grant number 075-15-2020-806 agreement dated 29 September 2020.

Informed Consent Statement: Not applicable.

Data Availability Statement: Not applicable.

Conflicts of Interest: The authors declare no conflict of interest.

Nomenclature

d	tube diameter, mm
L	tube length, m
l	integral scale of longitudinal structures, mm
U	instantaneous velocity, m/s
U_b	bulk gas velocity in the tube, m/s
U_{cl}	axial gas velocity at a given cross-section, m/s
U_m	axial gas velocity at the tube outlet, m/s
U_r	gas velocity in radial direction, m/s
W	instantaneous velocity vector, m/s
u	root-mean-square of velocity fluctuations, m/s
r	radial coordinate, mm
t	time, s
T	temperature, °C
$Tu = u/U_m \times 100\%$	turbulence level, %
x	longitudinal coordinate, mm
x_1	coordinate of the laminar-turbulent transition in the jet, mm
$P = l_t / \delta_L$	linear scale ratio
$R(\tau)$	Eulerian time-correlation function determined from longitudinal velocity pulsations
$Re = U_b d / \nu$	Reynolds number
Re_{cr}	critical Reynolds number
Re_1	lower boundary of the laminar-turbulent transition
Re_2	top boundary of the laminar-turbulent transition
$Ri = \Delta \rho g l / (\rho_0 U_b^2)$	Richardson number
$S = \frac{u}{S_L}$	characteristic velocity ratio
$t^* = \int_0^\infty R\left(\frac{\tau U_{cl}}{d}\right) d\left(\frac{\tau U_{cl}}{d}\right)$	Eulerian integral time scale
γ	intermittency factor
δ	thickness of the shear layer, mm
τ	autocorrelation function time lag, s
ω	vorticity, 1/s

References

1. Crow, S.C.; Champagne, F.H. Orderly structure in jet turbulence. *J. Fluid Mech.* **1971**, *48*, 547–591. [[CrossRef](#)]
2. Brown, G.L.; Roshko, A. On density effects and large structure in turbulent mixing layers. *J. Fluid Mech.* **1974**, *64*, 775–816. [[CrossRef](#)]
3. Ball, C.G.; Fellouah, H.; Pollard, A. The flow field in turbulent round free jets. *Prog. Aerosp. Sci.* **2012**, *50*, 1–26. [[CrossRef](#)]
4. Brown, G.L.; Roshko, A. Turbulent shear layers and wakes. *J. Turbul.* **2012**, *13*, N51. [[CrossRef](#)]
5. Ho, C.M.; Huerre, P. Perturbed Free Shear Layers. *Ann. Rev. Fluid Mech.* **1984**, *16*, 365–422. [[CrossRef](#)]
6. Michalke, A. Survey on jet instability theory. *Prog. Aerosp. Sci.* **1984**, *21*, 159–199. [[CrossRef](#)]
7. Ginevsky, A.S.; Vlasov, Y.V.; Karavosov, R.K. *Acoustic Control of Turbulent Jets*; Springer: Berlin, Germany, 2004. [[CrossRef](#)]

8. Nogueira, P.A.S.; Cavalieri, A.V.G.; Jordan, P.; Jaunet, V. Large-scale streaky structures in turbulent jets. *J. Fluid Mech.* **2019**, *873*, 211–237. [[CrossRef](#)]
9. Hussain, A.K.M.F.; Zaman, K.B.M.Q. The ‘preferred mode’ of the axisymmetric jet. *J. Fluid Mech.* **1981**, *110*, 39–71. [[CrossRef](#)]
10. Abiev, R.S.; Sirotkin, A.A. Influence of hydrodynamic conditions on micromixing in microreactors with free impinging jets. *Fluids* **2020**, *5*, 179. [[CrossRef](#)]
11. Van Hout, R.; Murugan, S.; Mitra, A.; Cukurel, B. Coaxial circular jets—A review. *Fluids* **2021**, *6*, 147. [[CrossRef](#)]
12. Chakchak, S.; Hidouri, A.; Zaidaoui, H.; Chrigui, M.; Boushaki, T. Experimental and numerical study of swirling diffusion flame provided by a coaxial burner: Effect of inlet velocity ratio. *Fluids* **2021**, *6*, 159. [[CrossRef](#)]
13. Takahashi, F.; Mizomoto, M.; Ikai, S. Transition from laminar to turbulent free jet diffusion flames. *Combust. Flame* **1982**, *48*, 85–95. [[CrossRef](#)]
14. Schumacher, J.; Eckhardt, B.; Haller, G. In Euromech colloquium 586: Turbulent superstructures in closed and open flows, 2017 Erfurt July 12–14, 2017, Erfurt, Germany. Available online: <https://586.euromech.org/> (accessed on 5 November 2021).
15. Duguet, Y. Intermittency in transitional shear flows. *Entropy* **2021**, *23*, 280. [[CrossRef](#)] [[PubMed](#)]
16. Hutchins, N.; Marusic, I.V.A.N. Evidence of very long meandering features in the logarithmic region of turbulent boundary layers. *J. Fluid Mech.* **2007**, *579*, 1–28. [[CrossRef](#)]
17. Li, W.J.; Zhang, Y.; Yang, B.; Su, J.W.; Zhang, Y.W.; Lu, W.Z.; Shui, Q.X.; Wu, X.Y.; He, Y.P.; Gu, Z.L. Large-scale turbulence structures in a laboratory-scale boundary layer under steady and gusty wind inflows. *Sci. Rep.* **2019**, *9*, 9373. [[CrossRef](#)] [[PubMed](#)]
18. Wygnanski, I.J.; Champagne, F.H. On transition in a pipe. Part 1. The origin of puffs and slugs and the flow in a turbulent slug. *J. Fluid Mech.* **1973**, *59*, 281–335. [[CrossRef](#)]
19. Avila, K.; Moxey, D.; Lozar, A.; Avila, M.; Barkley, D.; Hof, B. The onset of turbulence in pipe flow. *Science* **2011**, *333*, 192–196. [[CrossRef](#)] [[PubMed](#)]
20. Mullin, T. Experimental studies of transition to turbulence in a pipe. *Ann. Rev. Fluid Mech.* **2011**, *43*, 1–24. [[CrossRef](#)]
21. Lemanov, V.V.; Lukashov, V.V.; Abdrakhmanov, R.K.; Arbuzov, V.A.; Dubnishchev, Y.N.; Sharov, K.A. Regimes of unstable expansion and diffusion combustion in a hydrocarbon fuel jet. *Combust. Explos. Shock Waves* **2018**, *54*, 255–263. [[CrossRef](#)]
22. Dubnishchev, Y.; Lemanov, V.; Lukashov, V.; Arbuzov, V.; Sharov, K. Chapter 3. Hydrodynamic vortex structures in a diffusion jet flame. In *Swirling Flows and Flames*; Boushaki, T., Ed.; Books on Demand: London, UK, 2019; pp. 33–54. [[CrossRef](#)]
23. Lemanov, V.V.; Lukashov, V.V.; Sharov, K.A. Transition to turbulence through intermittence in inert and reacting jets. *Fluid Dyn.* **2020**, *55*, 768–777. [[CrossRef](#)]
24. Meyer, J.P.; Everts, M.; Coetzee, N.; Grote, K.; Steyn, M. Heat transfer coefficients of laminar, transitional, quasi-turbulent and turbulent flow in circular tubes. *Int. Comm. Heat Mass Trans.* **2019**, *105*, 84–106. [[CrossRef](#)]
25. Cerbus, R.T.; Chien-chia, L.; Gustavo, G.; Pinaki, C. Small-scale universality in the spectral structure of transitional pipe flows. *Sci. Adv.* **2021**, *6*, eaaw6256. [[CrossRef](#)] [[PubMed](#)]
26. Barker, S.J.; Gile, D. Experiments on heat-stabilized laminar boundary layers in water. *J. Fluid Mech.* **1981**, *104*, 139–158. [[CrossRef](#)]
27. Renard, P.-H.; Thévenin, D.; Rolon, J.C.; Candel, S. Dynamics of flame/vortex interactions. *Prog. Eng. Combust. Sci.* **2000**, *26*, 225–282. [[CrossRef](#)]
28. Manu, K.V.; Anand, P.; Chetia, U.K.; Basu, S. Effects of instabilities and coherent structures on the performance of a thermocline based thermal energy storage. *Appl. Therm. Eng.* **2015**, *87*, 768–778. [[CrossRef](#)]
29. Savitskii, A.; Lobasov, A.; Sharaborin, D.; Dulin, V. Testing basic gradient turbulent transport models for swirl burners using PIV and PLIF. *Fluids* **2021**, *6*, 383. [[CrossRef](#)]
30. Westerweel, J.; Fukushima, C.; Pedersen, J.M.; Hunt, J.C.R. Mechanics of the turbulent-nonturbulent interface of a jet. *Phys. Rev. Lett.* **2005**, *95*, 174501. [[CrossRef](#)]
31. Gampert, M.; Narayanaswamy, V.; Schaefer, P.; Peters, N. Conditional statistics of the turbulent/non-turbulent interface in a jet flow. *J. Fluid Mech.* **2013**, *731*, 615–638. [[CrossRef](#)]
32. Kuan, C.L.; Wang, T. Investigation of the intermittent behavior of transitional boundary layer using a conditional averaging technique. *Exp. Therm. Fluid Sci.* **1990**, *3*, 157–173. [[CrossRef](#)]
33. Lemanov, V.V.; Terekhov, V.I.; Sharov, K.A.; Shumeiko, A.A. An experimental study of submerged jets at low Reynolds numbers. *Tech. Phys. Lett.* **2013**, *39*, 421–423. [[CrossRef](#)]
34. Pomeau, Y.; Manneville, P. Intermittent transition to turbulence in dissipative dynamical systems. *Comm. Math. Phys.* **1980**, *74*, 189–197. [[CrossRef](#)]
35. Eckhardt, B.; Schneider, T.M. How does flow in a pipe become turbulent? *Eur. Phys. J. B* **2008**, *64*, 457–462. [[CrossRef](#)]
36. Couliou, M.; Monchaux, R. Large-scale flows in transitional plane Couette flow: A key ingredient of the spot growth mechanism. *Phys. Fluids* **2015**, *27*, 034101. [[CrossRef](#)]
37. Meyer, T.R.; Fiechtner, G.J.; Gogineni, S.P.; Rolon, J.C.; Carter, C.D.; Gord, J.R. Simultaneous PLIF/PIV investigation of vortex-induced annular extinction in H₂-air counter flow diffusion flames. *Exp. Fluids* **2004**, *36*, 259–267. [[CrossRef](#)]
38. Takeno, T.; Kotani, Y. Transition and structure of turbulent jet diffusion flames. *Prog. Astronaut. Aeronaut.* **1978**, *58*, 19–35. [[CrossRef](#)]
39. Chung, S.H.; Lee, B.J. On the characteristics of laminar lifted flames in a nonpremixed jet. *Combust. Flame* **1991**, *86*, 62–72. [[CrossRef](#)]

-
40. Linan, A.; Vera, M.; Sanchez, A.L. Ignition, liftoff, and extinction of gaseous diffusion flames. *Annu. Rev. Fluid Mech.* **2015**, *47*, 293–314. [[CrossRef](#)]
 41. Kurbatskii, A.F.; Kurbatskaya, L.I. RANS modelling of intermittent turbulence in a thermally stable stratified boundary layer. *J. Appl. Mech. Tech. Phys.* **2013**, *54*, 561–571. [[CrossRef](#)]
 42. Hallberg, M.P.; Strykowski, P.J. On the universality of global modes in low-density axisymmetric jets. *J. Fluid. Mech.* **2006**, *569*, 493–507. [[CrossRef](#)]